Excitation-inhibition imbalance in Alzheimer's disease using multiscale neural model inversion of resting-state fMRI

Guoshi Li[1, 2], Li-Ming Hsu[2, 3], Ye Wu[1, 2], Andrea C Bozoki [3], Yen-Yu Ian Shih[2, 3], Pew-Thian Yap[1, 2] *

[1] Department of Radiology
University of North Carolina
Chapel Hill, NC USA

[2] Biomedical Research Imaging Center
University of North Carolina
Chapel Hill, NC USA

[3] Department of Neurology
University of North Carolina
Chapel Hill, NC, USA

*Correspondence: ptyap@med.unc.edu

Abstract

Alzheimer's disease (AD) is a serious neurodegenerative disorder without a clear understanding of the etiology and pathophysiology. Recent experimental data has suggested excitation-inhibition (E-I) imbalance as an essential element and critical regulator of AD pathology, but E-I imbalance has not been systematically mapped out in both local and large-scale neuronal circuits in AD. Using a multiscale neural model inversion framework, we identified disrupted E-I balance as well as impaired excitatory and inhibitory connections in a large network during AD progression based on resting-state functional MRI data from the Alzheimer's Disease Neuroimaging Initiative (ADNI) database. We observed that E-I balance is progressively disrupted from mild cognitive impairment (MCI) to AD and alteration of E-I balance is bidirectional varying from region to region. Also, we found that inhibitory connections are more significantly impaired than excitatory connections and the strength of the majority of excitatory and inhibitory connections reduces in MCI and AD, leading to gradual decoupling of neural populations. Moreover, we revealed a core AD network comprising mainly of limbic and cingulate regions including the hippocampus, pallidum, putamen, nucleus accumbens, inferior temporal cortex and caudal anterior cingulate cortex. These brain regions exhibit consistent and stable E-I alteration across MCI and AD, which may represent a stable AD biomarker and an important therapeutic target. Overall, our study constitutes the first attempt to delineate E-I imbalance in large-scale neuronal circuits during AD progression, which facilitates the development of new treatment paradigms to restore pathological E-I balance in AD.

Introduction

Alzheimer's disease (AD) is neurodegenerative disorder characterized by progressive and irreversible cognitive decline (Bateman et al., 2012). It is the leading cause of dementia affecting more than 47 million people worldwide and this number is expected to increase to 131 million by 2050 (Tiwari et al., 2019). The healthcare cost for patients with AD and other dementias is enormous and is estimated to be 236 billion in the US for 2016 alone and predicted to quadruple by 2050 (Alzheimer's Association, 2016). Despite decades of extensive research, a clear understanding of the etiology and pathophysiology of AD remains elusive. Current treatments are only symptomatic without slowing down the progression of the disease (Aldehri et al., 2018). The lack of effective treatment highlights the paramount importance of identifying new pathophysiological and therapeutic targets (Thakur et al., 2018).

Excitation-inhibition (E-I) balance represents a promising pathophysiological and therapeutic target for AD. First, disrupted E-I balance may underlie the key pathophysiological mechanism of AD. One of the pathological hallmarks of AD is the accumulation of amyloid-β (Aβ) peptides in the brain that occurs long before clinical disease onset (Karran et al., 2011; Huang and Mucke, 2012). During this long extended preclinical stage, soluble Aβ oligomers and amyloid plaques disrupt neuronal circuit activity and function by altering synaptic transmission and E-I balance leading to cognitive malfunction (Palop and Mucke, 2010; Busche and Konnerth, 2016; Palop and Mucke, 2016). In particular, high Aβ levels elicit epileptiform discharges and non-convulsive seizures in both hippocampal and neocortical networks of human amyloid precursor protein (hAPP) transgenic mice (Palop et al., 2007), which closely relates to the increased incidence of epileptic seizures in AD patients (Palop and Mucke, 2009). Second, E-I disruption is not only the consequence of Aβ deposit, but also the driver of the amyloid pathology. Experimental data indicate that Aβ release is regulated by neuronal activity (Nitsch et al., 1993; Bero et al., 2011) and driven by increased metabolism (Cohen et al., 2009; Johnson et al., 2014). Also, Aβ accumulation is associated with enhanced neural activity in task-related regions during memory encoding (Mormino et al., 2012) and

reduction of neural hyperactivity decreases Aβ aggregation as well as axonal dystrophy and synaptic loss (Yuan and Grutzendler, 2016). Lastly, restoration of E-I balance has been shown to rescue circuit dysfunction and ameliorate cognitive impairments in both AD mouse models (Verret et al., 2012; Busche et al., 2015; Yuan and Grutzendler, 2016) and human with early AD (Bakker et al., 2012), suggesting a direct link between E-I imbalance and cognitive malfunction. Taken together, these findings highlight the paramount importance of identifying E-I imbalance in AD, particularly in the initial disease stage for early diagnosis and intervention.

Functional magnetic resonance imaging (fMRI) is a core noninvasive method to measure brain activity (Glover, 2011) and has been widely used to study functional network alterations in AD (Filippi and Agosta, 2011; Brier et al., 2014; Dennis and Thompson, 2014). These studies have revealed both abnormal brain network activation/deactivation and dysfunctional connectivity patterns in AD. Specifically, a number of studies have reported deficit task-induced deactivation in the default mode network (DMN) (Lustig et al., 2003; Greicius et al., 2004; Rombouts et al., 2005), a collection of brain regions which are deactivated during cognitive tasks and implicated in internal mentation and episodic memory (Raichle et al., 2001; Fox and Raichle, 2007). Notably, such abnormal deactivation pattern is increasingly compromised over the course of AD from normal aging to amnestic mild cognitive impairment (aMCI) and to AD (Pihlajamäki and Sperling, 2009). As the core region of the memory network, the hippocampus (HPC) shows elevated activation in patients with aMCI, but reduced activation in patients with late aMCI and AD (Dickerson et al., 2004, 2005; Celone et al., 2006). In addition to abnormal functional network activation/deactivation, AD has been recognized as a disease of dysfunctional connectivity (Delbeuck et al., 2003; Stam et al., 2007; Wang et al., 2007; Supekar et al., 2008; Sanz-Arigita et al., 2010). Studies using seed-based approach or independent component analysis (ICA) have observed widespread decrease in functional connectivity (FC) in both aMCI and symptomatic AD within the DMN including the bilateral precuneus/posterior cingulate cortex (PCC), medial prefrontal

cortex (mPFC), lateral temporal cortex and inferior parietal cortex (Sorg et al., 2007; Bai et al., 2009; Zhang et al., 2009; Qi et al., 2010; Brier et al., 2012). Consistently, other seed-based studies have reported reduced connectivity between the HPC and multiple DMN regions including the PCC, lateral temporal cortex and mPFC (Wang, et al, 2006; Allen, 2007). In addition to decreased FC, increased FC has also been observed in AD. A number of studies have reported that AD is associated with increased FC between the HPC and prefrontal cortex (PFC) (Wang et al., 2006), and between DMN regions and PFC (Bai et al., 2009; Zhang et al., 2009; Qi et al., 2010), suggesting enhanced PFC connectivity may compensate for the reduced temporal function (Filippi and Agosta, 2011). Using graph theory analysis, Supekar et al. (2008) reported both abnormally decreased and increased FC in the entire brain, consistent with a high-dimensional seed-based analysis method that found diverse FC impairments in AD (Wang et al., 2007). Aberrant FC pattern changes also depend on the specific AD progression stage. Brier et al., (2012) demonstrated increased FC in the salience network and decreased FC in the DMN, executive control and sensori-motor networks at the very mild AD stage, while all networks displayed reduced FC at the mild-moderate AD stage.

Despite the great success of conventional fMRI analysis in characterizing altered network activation and connectivity patterns in AD, they are not able to identify E-I imbalance at circuit level because such statistical tools do not allow for determination of causal relationships between regions, nor do they provide insight into the dynamic meso-scale neuronal relationships that underpin BOLD signal variations. In contrast, generative modeling-based fMRI analysis has the capability of both inferring E-I balance at circuit level and simulating the impact of E-I imbalance on network dynamics (Li and Yap, 2022). For example, de Hann et al. (2012, 2017) developed a large-scale neural mass model to examine the effects of excessive neuronal activity on functional network topology and dynamics. In the first study (de Hann et al., 2012), they demonstrated that synaptic degeneration induced by neuronal hyperactivity resulted in hub vulnerability in AD including loss of spectral power and long-range synchronization. In a subsequent

study (de Hann et al., 2017), paradoxically, the authors found that selective stimulation of all excitatory neurons in the network led to sustained preservation of network integrity in the presence of activity-dependent synaptic degeneration. Using a computational framework termed "The Virtual Brain (TVB)", Zimmerman et al., (2018) estimated personalized local excitation and inhibition parameters as well as global coupling strength based on resting-state fMRI (rs-fMRI) data from healthy individuals and patients with aMCI and AD. They demonstrated that the model parameters required to accurately simulate empirical FC significantly correlated with cognitive performance, which surpassed the predictive capability of empirical connectomes. However, these studies focused on network simulation and AD differentiation rather than E-I estimation. In addition, these models used structural connectivity (SC) as a proxy for synaptic efficiency, assumed the same local kinetic parameters for all regions and estimated only one global scaling coefficient for all long-range inter-regional connections, which cannot infer region-specific E-I imbalance in AD.

The goal of this study is to identify region-specific E-I imbalance during the progression of AD. Towards this aim, we apply a recently developed computational framework termed "Multiscale Neural Model Inversion (MNMI)" (Li et al., 2019; 2021) to the resting-state fMRI (rs-fMRI) data obtained from the Alzheimer's Disease Neuroimaging Initiative (ADNI) database consisting of normal aging subjects and individuals with MCI and AD. The strengths of MNMI include using a biologically plausible neural mass model to describe network dynamics, estimating both intra-regional and inter-regional effective connectivity (EC), and constrain EC estimation with structural information. Specifically, MNMI estimates region-specific local recurrent excitation and inhibition coupling weight as well as individual inter-regional connection strength at single subject level based on rs-fMRI, enabling the inference of region-specific E-I balance. We first estimated individual connection strength for all subjects and then derived both intra-regional (local) and inter-regional (external) E-I balance from estimated EC. Using statistical analysis, we characterized both altered excitatory/inhibitory interactions among neural populations and

disrupted intra-regional/inter-regional E-I balance in MCI and AD. This computational study offers mechanistic insights into systematic alteration in E-I balance during AD progression, which facilitates the development of new diagnostic technique and new treatment paradigm to specifically detect and modulate E-I imbalance in AD.

Methods

Overview of MNMI

The schematic diagram of the MNMI framework is depicted in Fig. 1. The neural activity (x) is generated by a neural mass network model (Wilson and Cowan, 1972) consisting of multiple brain regions (R1, R2, etc.). Each region contains one excitatory (E) and one inhibitory (I) neural population coupled with reciprocal connections and receives spontaneous input (u). Different brain regions are connected via long-range fibers whose baseline strengths are determined by SC from diffusion MRI and weak inter-regional connections are removed to avoid over-parameterization. The neural activity (x) is converted to BOLD signals (y) via convolution with a hemodynamic response function (HRF, Friston et al., 1998). Both intra-regional recurrent excitation (W_{EE}) and inhibition (W_{IE}) weights and inter-regional connection strengths (W_{12}, W_{21}, etc.) as well as spontaneous input (u) are estimated using genetic algorithm to minimize the difference between simulated and empirical FC.

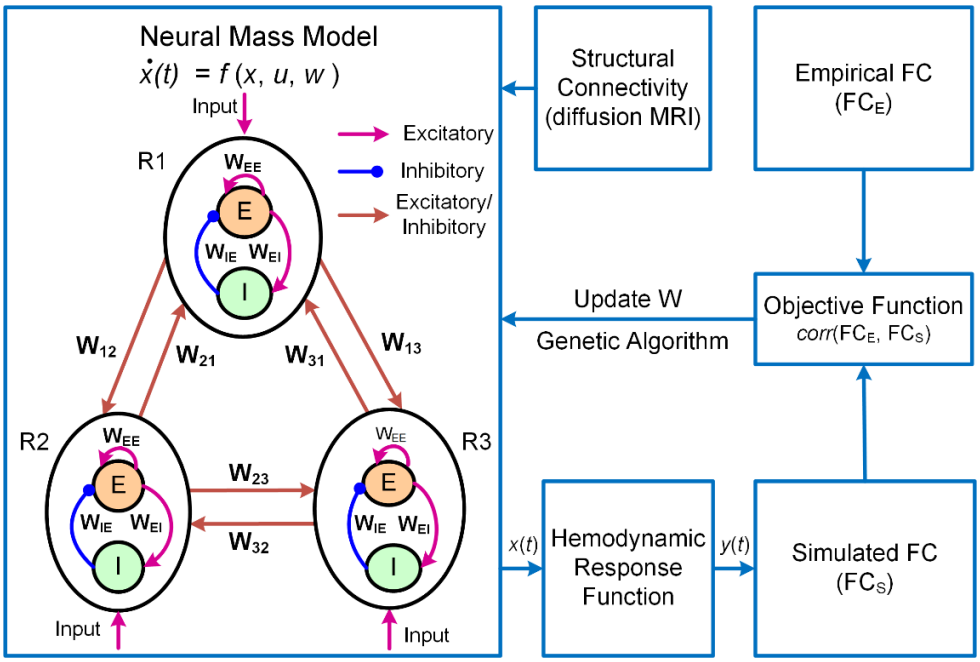

Figure 1. Overview of the MNMI framework. The neural activity (x) is described by a neural mass network model containing multiple brain regions (R1, R2, etc.). Each region consists of one excitatory (E) and one inhibitory (I) neural population coupled with reciprocal connections. Inter-regional connection strength is based on SC from diffusion MRI. The neural activity (x) is converted to corresponding BOLD signals (y) via a hemodynamic response function. The model parameters are optimized to minimize the difference between simulated FC and empirical FC.

Subjects

The rs-fMRI data (baseline scans) was obtained from the ADNI dataset (http://adni.loni.usc.edu/). A total of 144 subjects with Mini-Mental State Examination (MMSE) scores were selected from the ADNI-Go and ADNI-2 studies, including 48 NC (25/23 males/females, age 73.1 ± 6.5 years, MMSE 29.1 ± 0.9), 48 MCI (25/23 males/females, age 74.3 ± 9.8 years, MMSE 27.9 ± 1.6) and 48 AD subjects (25/23 males/females, age 73.3 ± 8.5 years, MMSE 23.1 ± 2.5). All subjects were matched in terms of age (p = 0.752, one-way Analysis of Variance (ANOVA)) and gender.

Image preprocessing

Data quality control was implemented in ADNI to ensure consistency across imaging centers in terms of the scanner, imaging protocol, and signal-to-noise ratio (Jack Jr et al., 2008). The fMRI data (7 min, 140 volumes) was preprocessed using AFNI (Cox, 1997) according to a well-accepted pipeline (Yan and Zang, 2010), which includes first ten volumes removal, head motion correction, normalization, nuisance signals regression, detrend and bandpass filtering (0.01 to 0.08 Hz). Nuisance regressors include head motion parameters (the "Friston-24" model), the mean BOLD signal of the white matter, and cerebrospinal fluid. To minimize artifacts due to excessive motion, the subjects with an average frame displacement (FD) (Power et al., 2014) greater than 0.5 mm will be removed. Finally, fMRI data will be smoothed with 6 mm full width at half maximum (FWHM) Gaussian kernel and then nonlinearly registered to the Montreal Neurological Institutes (MNI) space.

Functional and structural connectivity

Regional averaged BOLD rs-fMRI time series were extracted using the Desikan-Killiany (DK) atlas (Desikan et al., 2006) with 84 regions of interest (ROIs). To reduce computational burden and focus on the networks that are most affected in AD (Zott et al., 2018), we selected 46 ROIs from the DMN, salience, executive control (frontoparietal control) and limbic networks (Table 1) based on Yeo's seven network definition (Yeo et al., 2011) and computed the individual FC matrix using Pearson's correlation.

Table 1. Region of interest (ROI) selected in network modeling.

Network	ROI	Abbreviation
Default Mode Network	Left inferior parietal cortex	L.IPC
	Right inferior parietal cortex	R.IPC
	Left isthmus cingulate cortex	L.ICC
	Right isthmus cingulate cortex	R.ICC
	Left middle temporal cortex	L.MTC
	Right middle temporal cortex	R.MTC
	Left precuneus	L.PCU
	Right precuneus	R.PCU
	Left rostral anterior cingulate cortex	L.rACC
	Right rostral anterior cingulate cortex	R.rACC
	Left superior frontal cortex	L.SFC
	Right superior frontal cortex	R.SFC
	Left superior temporal cortex	L.STC
	Right superior temporal cortex	R.STC
	Left posterior cingulate cortex	L.PCC
	Right posterior cingulate cortex	R.PCC
Salience Network	Left caudal anterior cingulate cortex	L.cACC
	Right caudal anterior cingulate cortex	R.cACC
	Left supramarginal gyrus	L.SMG
	Right supramarginal gyrus	R.SMG
	Left insula	L.IN
	Right insula	R.IN
Executive Control Network	Left caudal middle frontal cortex	L.cMFC
	Right caudal middle frontal cortex	R.cMFC
	Left rostral middle frontal cortex	L.rMFC
	Right rostral middle frontal cortex	r.rMFC
	Left superior parietal cortex	L.SPC
	Right superior parietal cortex	R.SPC
Limbic Network	Left entorhinal cortex	L.ETC
	Right entorhinal cortex	R.ETC
	Left inferior temporal cortex	L.ITC
	Right inferior temporal cortex	R.ITC
	Left thalamus	T.THAL
	Right thalamus	R.THAL
	Left caudate	L.CA
	Right caudate	R.CA
	Left putamen	L.PUT
	Right putamen	R.PUT
	Left pallidum	L.PAL
	Right pallidum	R.PAL
	Left hippocampus	L.HPC
	Right hippocampus	R.HPC
	Left amygdala	L.AMY
	Right amygdala	R.AMY
	Left nucleus accumbens	L.ACB
	Right nucleus accumbens	R.ACB

Structural connectivity was computed using probabilistic tractography based on the diffusion MRI data consisting of 100 unrelated subjects from the WU-Minn Human Connectome Project (HCP) young healthy adults, 1200 subjects release (Van Essen et al., 2013). The diffusion MRI data have been preprocessed using the HCP protocols. To compute SC, we conducted whole-brain tractography using asymmetry spectrum imaging (ASI) fiber tracking which fits a mixture of asymmetric fiber orientation distribution functions (AFODFs) to the diffusion signal (Wu et al., 2019, 2020). White matter streamlines were generated by successively following local directions determined from the AFODFs. The output streamlines were cropped at the grey/white-matter interface with a search distance of 2 mm, where the DK atlas was applied to obtain 84×84 SC matrix. The reduced SC matrix with 46 ROIs was extracted from the full SC matrix and averaged among the 100 subjects followed by normalization so the SC was bounded between 0 and 1. Finally, we selected the strongest 10% SC connections for network modeling and the weaker connections were removed (Frässle et al., 2017; Li et al., 2021).

Neural mass model and hemodynamic response

We employed computational neuronal modeling to capture the neural interactions and dynamics in the AD network. The regional brain dynamics was simulated by a neural mass model using the biologically motivated nonlinear Wilson-Cowan oscillator (Wilson and Cowan, 1972). The population-level activity of the j^{th} region was governed by the following equations (Abeysuriya et al., 2018; Li et al., 2011):

$$\tau_e \frac{dE_j(t)}{dt} = -E_j(t) + S\left(\sum_k W_{kj} C_{kj} E_k(t) + W_{EE}^j E_j(t) - W_{IE}^j I_j(t) + u + \varepsilon(t)\right) \quad (1)$$

$$\tau_i \frac{dI_j(t)}{dt} = -I_j(t) + S\left(W_{EI}^j E_j(t) + \varepsilon(t)\right) \quad (2)$$

where E_j and I_j are the mean firing rates of excitatory and inhibitory neural populations in brain region j, τ_e and τ_i are the excitatory and inhibitory time constants (20 ms; Hellyer et al., 2016), and W_{EE}^j, W_{IE}^j and W_{EI}^j are the local coupling strengths (i.e., recurrent excitation, recurrent inhibition and excitatory to inhibitory weight). The variable u is a constant spontaneous input and $\varepsilon(t)$ is random additive noise

following a normal distribution (Deco et al., 2013; Wang et al., 2019). The long-range connectivity strength from region *k* to region *j* is represented by W_{kj} which is scaled by empirical SC (C_{kj}), and the nonlinear response function *S* is a sigmoid function $= 1/(1 + e^{-(\frac{x-\mu}{\sigma})})$ (μ=1.0; σ =0.25; Abeysuriya et al., 2018).

To increase computational efficiency, we replaced the hemodynamic state equations in the original MNMI model (Li et al., 2021) with the canonical HRF and computed the hemodynamic response as the convolution of regional neural activity and the SPM-style HRF kernel (Friston et al., 1998):

$$h(t) = \frac{t^{\alpha_1 - 1}\beta_1{}^{\alpha_1} e^{-\beta_1 t}}{\Gamma(\alpha_1)} - c\frac{t^{\alpha_2 - 1}\beta_2{}^{\alpha_2} e^{-\beta_2 t}}{\Gamma(\alpha_2)} \quad (3)$$

where *t* indicates time, $\alpha_1 = 6$, $\alpha_2 = 16$, $\beta_1 = \beta_2 = 1$, $c = 1/6$, and Γ represents the gamma function. The regional neural activity was calculated as the weighted sum of excitatory and inhibitory neural activity (i.e., $x_j = \frac{2}{3}E_j + \frac{1}{3}I_j$; Becker et al., 2015; Li et al, 2021).

Estimation of model parameters

Both local (intra-regional) and long-range (inter-regional) connection strengths in the model were estimated. For the local parameters, we estimated both recurrent excitation (W_{EE}) and recurrent inhibition (W_{IE}) weights in each ROI, resulting in 92 local parameters. The E→I coupling weight (W_{EI}) was assumed to be constant (3.0; Li et al., 2021) as the effect of W_{EI} could be accommodated by change in W_{IE}. To avoid over-parameterization and false positive connections due to DTI noise, we estimated the strongest 10% inter-regional connections (N = 212) and removed the remaining weaker connections. In addition, the spontaneous input (u) was also estimated, which resulted in a total of 305 free parameters for estimation.

We used the genetic algorithm (GA; implemented by the *ga* function in MATLAB global optimization toolbox) to estimate the model parameters. The parameters were bounded within certain ranges to achieve balanced excitation and inhibition in the network (Li et al., 2021): W_{EE} and $W_{IE} \in [2, 4]$, $W_{ki} \in [-2, 2]$, and $u \in [0.2, 0.4]$. GA maximized the Pearson's correlation between the simulated and empirical FC

matrices with the functional tolerance set to be 1e-3 and the maximal number of generations set to be 128. We observed good convergence within 128 generations for all the subjects.

Numerical integration

The differential equations of the neural mass model were simulated using the 4th order Runge-Kutta (RK) scheme with an integration step of 10 ms; shorter integration step has no significant effect on the results reported. We simulated the network for a total of 200 sec, and the first 20 sec of the BOLD activity was discarded to remove transient effects. The remaining 180 sec time series were downsampled to 0.33 Hz to have the same temporal resolution as the empirical BOLD signals (TR = 3 sec). The model along with the optimization procedure were coded in MATLAB and run in parallel with 24 cores in a high-performance UNC Linux computing cluster. The typical computing time (for each individual subject) ranged from 20 to 30 hours.

Statistical analysis

Model parameters were estimated for each subject and compared between NC and MCI, and between NC and AD. We used two-sample *t*-tests to compare local and inter-regional connection strengths as well as intra-regional and inter-regional E-I balance. Multiple comparisons were corrected by either the false discovery rate (FDR) or the Network-based Statistics (NBS; Zalesky et al., 2010) approach ($p < 0.05$).

Results

MNMI performance

The performance of MNMI is illustrated in Fig. 2. The GA converged within 128 generations for all 144 subjects and the convergence time ranged from 20 to 30 hours with 24 computing cores. The average fitness value (Pearson's correlation between simulated and empirical FC) was 0.61 for both the NC and MCI groups, and 0.62 for the AD group. Both the simulated neural activity and BOLD signals displayed rhythmic fluctuations (Fig. 2A, B). The oscillation frequency of the neural activity was about 7-10 Hz, consistent with α oscillations during relaxed wakefulness (Hughes and Crunelli, 2005). The frequency of the BOLD signals ranged between 0.01 and 0.05 Hz, in line with experimental observation (Tong et al., 2019). The empirical and simulated FC are displayed in Fig. 2C, D respectively. It is noted that the pattern of the simulated FC closely matched that of the empirical FC.

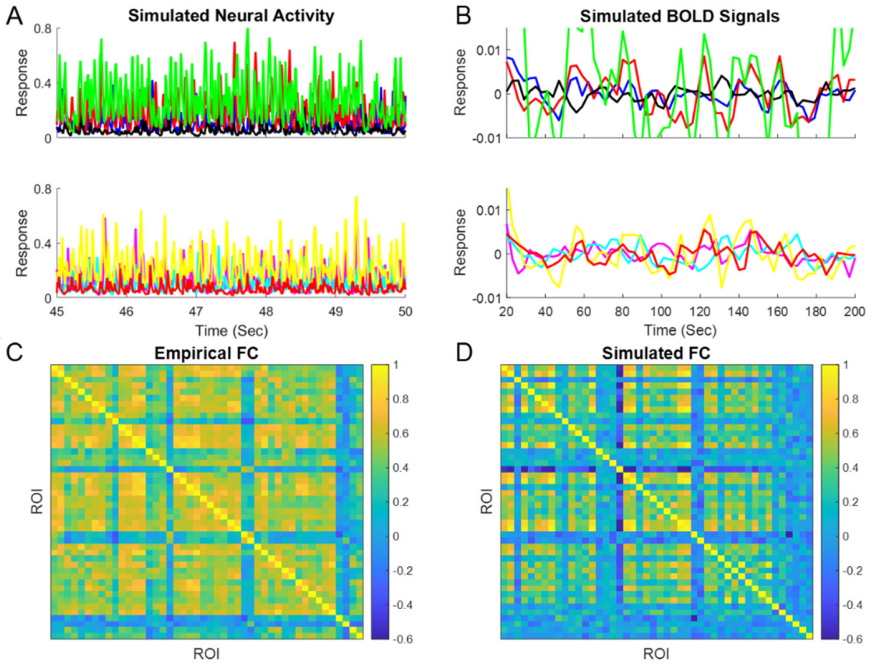

Figure 2. Performance of MNMI. (A) Sample activity of excitatory neural populations in eight randomly selected ROIs (four in top and four in bottom). **(B)** Sample BOLD signals in the same eight ROIs. **(C)** Empirical FC from a randomly selected subject. **(D)** Simulated FC from the same subject.

Disrupted intra-regional E-I balance in MCI and AD

We first examined whether intra-regional (local) E-I balance was altered in MCI and AD. The recurrent excitation and inhibition weights within 46 ROIs are shown in Fig. 3A for NC and MCI, and Fig. 3B for NC and AD, respectively. We observed that compared to NC, three regions (R.IPC, L.rACC and R.cACC) showed marginally significant decrease ($p < 0.05$, uncorrected), while the other three regions (R.ETC, L.PAL and R.ACB) showed marginally significant increase ($p < 0.05$, uncorrected) for recurrent excitation in MCI (Fig. 3A1). In AD, six regions also displayed significant difference in recurrent excitation compared to NC, including L.cMFC, R.PAL, L.HPC and L.AMY with decreased excitation, and L.PCC and R.ACB with increased excitation (Fig. 3B1). Note that the significant excitation increase in R.ACB survived multiple correction ($p < 0.05$, corrected) and R.ACB was the only region that showed significant and consistent excitation change across MCI and AD. Both MCI and AD also showed significant difference in recurrent inhibition compared to NC. In MCI, the recurrent inhibition weight of five regions (L.cMFC, R.SPC, R.ITC, L.PAL and R.ACB) was significantly decreased ($p < 0.05$) while one region (L.SFC) showed significant increase ($p < 0.05$; Fig. 3A2). In particular, the change in L.cMFC survived multiple correction. In AD, the change in recurrent inhibition was much more pronounced than MCI (Fig. 3B2). Specifically, eleven ROIs exhibited significant difference in AD compared to NC where change in seven ROIs passed multiple correction. The recurrent inhibition of R.ICC, L.PCU, R.rACC, L.PCC, L.cMFC, R.SPC, R.ITC and L.PAL was significantly reduced, while that of L.SFC, R.cACC and L.HPC was significantly increased in AD. The regions that survived multiple correction included R.ICC, R.cACC, L.cMFC, R.SPC, R.ITC, L.PAL and L.HPC (Fig. 3B2, marked by double pink star). Notably, five ROIs showed consistent change in recurrent inhibition across MCI and AD (compare Fig. 3A2 with Fig. 3B2), including L.SFC, L.cMFC, R.SPC, R.ITC and L.PAL. Importantly, the difference in R.SPC, R.ITC and L.PAL was only marginally significant in MCI, which evolved to survive multiple correction in AD, suggesting more disruption of excitatory/inhibitory interactions in AD.

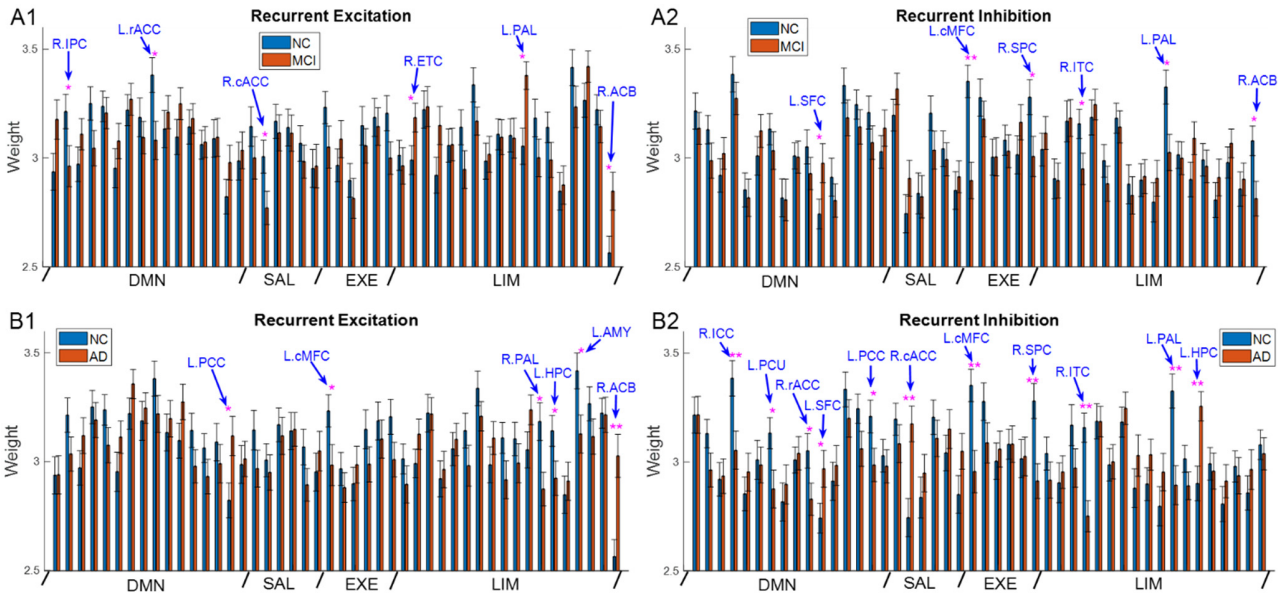

Figure 3. Impaired recurrent excitation and inhibition in MCI and AD. (A1) Comparison of average recurrent excitation weight between NC and MCI. **(A2)** Comparison of average recurrent inhibition weight between NC and MCI. **(B1)** Comparison of average recurrent excitation weight between NC and AD. **(B2)** Comparison of average recurrent inhibition weight between NC and AD. One star indicates uncorrected significance ($p < 0.05$) and double stars indicate corrected significance by FDR ($p < 0.05$). DMN: default mode network, SAL: salience network, EXE: executive control network, LIM: limbic network. Error bars indicate standard errors. The notations are the same for figures below.

To visualize the alterations in recurrent excitation and inhibition better, we listed the significant changes in MCI and AD in Table 2 where the red up arrow indicates significant increase while the green down arrow indicates significant decrease. Several observations can be made. First, more connections with more significant difference were compromised in AD than MCI. This is to be expected as AD represents a more severe disease stage than MCI. Second, the strength of the majority of connections (69%) was decreased in MCI/AD compared with NC. This is consistent with the widespread decrease in FC during the progression of AD (Filippi and Agosta, 2011; Brier et al., 2014; Dennis and Thompson, 2014). Third, if a region exhibited impairments in both recurrent excitation and inhibition, their directions of change were opposite to each other thus strengthening E-I imbalance, except for the executive control network where recurrent excitation and recurrent inhibition changed in the same direction. This suggests that there may exist certain compensatory mechanisms in the executive control network to maintain

similar E-I balance in the presence of AD pathology due to the critical role of this network in cognitive function (Miller et al., 2001; Petrides, 2005; Koechlin and Summerfield, 2007). Lastly, recurrent inhibition is more significantly disrupted by MCI/AD than recurrent excitation, in agreement with the emerging viewpoint of interneuron dysfunction in network impairments (Li et al., 2016; Palop and Mucke, 2016; Xu et al., 2020). The consistent impairments across MCI and AD may also suggest that inhibitory connections are more stable biomarkers of AD.

Table 2. Alterations in recurrent excitation and inhibition in MCI and AD. One star indicates uncorrected significance and double stars indicate corrected significance by FDR.

Network	ROI	MCI		AD	
		Excitation	Inhibition	Excitation	Inhibition
DMN	Inferior parietal (right)	* ↓			
	Isthmus cingulate (right)				* *↓
	Precuneus (left)				* ↓
	Rostral ACC (left)	* ↓			
	Rostral ACC (right)				* ↓
	Superior frontal (left)		* ↑		* ↑
	Posterior cingulate (left)			* ↑	* ↓
SAL	Caudal ACC (right)	* ↓			* *↑
EXE	Caudal middle frontal (left)		* *↓	* ↓	* *↓
	Superior parietal (right)		*↓		* *↓
LIM	Ectorhinal cortex (right)	* ↑			
	Inferior temporal (right)		* ↓		* *↓
	Pallidum (left)	* ↑	* ↓		* *↓
	Pallidum (right)			* ↓	
	Hippocampus (left)			* ↓	* *↑
	Amygdala (left)			* ↓	
	Accumbens (right)	* ↑	* ↓	* *↑	

The alteration in recurrent excitation and inhibition strengths resulted in intra-regional E-I imbalance in MCI and AD as shown in Fig. 4. The intra-regional (local) E-I balance was quantified as the net EC (i.e., recurrent excitation strength – recurrent inhibition strength). In MCI, three regions showed significant decrease in intra-regional E-I balance without passing multiple correction, including L.rACC, R.cACC and L.HPC (Fig. 4A). Three other regions in the limbic network displayed significant increase in

intra-regional E-I balance, including R.ITC, L.PAL and R.ACB, among which the elevation within L.PAL and R.ACB passed multiple correction. In AD, five regions showed consistent E-I impairments as MCI, including R.cACC, R.ITC. L.PAL, L.HPC and R.ACB (Fig. 4B). In particular, the E-I alteration in R.cACC and L.HPC became more significant in AD than MCI, surviving multiple correction. In addition to the five common ROIs, the intra-regional E-I balance in L.PCU, L.PCC, L.PUT and L.AMY were also impaired in AD, with significant increase in L.PCU and L.PCC, and significant decrease in L.PUT and L.AMY ($p < 0.05$); the increase in L.PCC was able to pass multiple correction ($p < 0.05$, corrected). Overall, the intra-regional E-I imbalance in MCI and AD was highly consistent and concentrated on the limbic network and cingulate cortex.

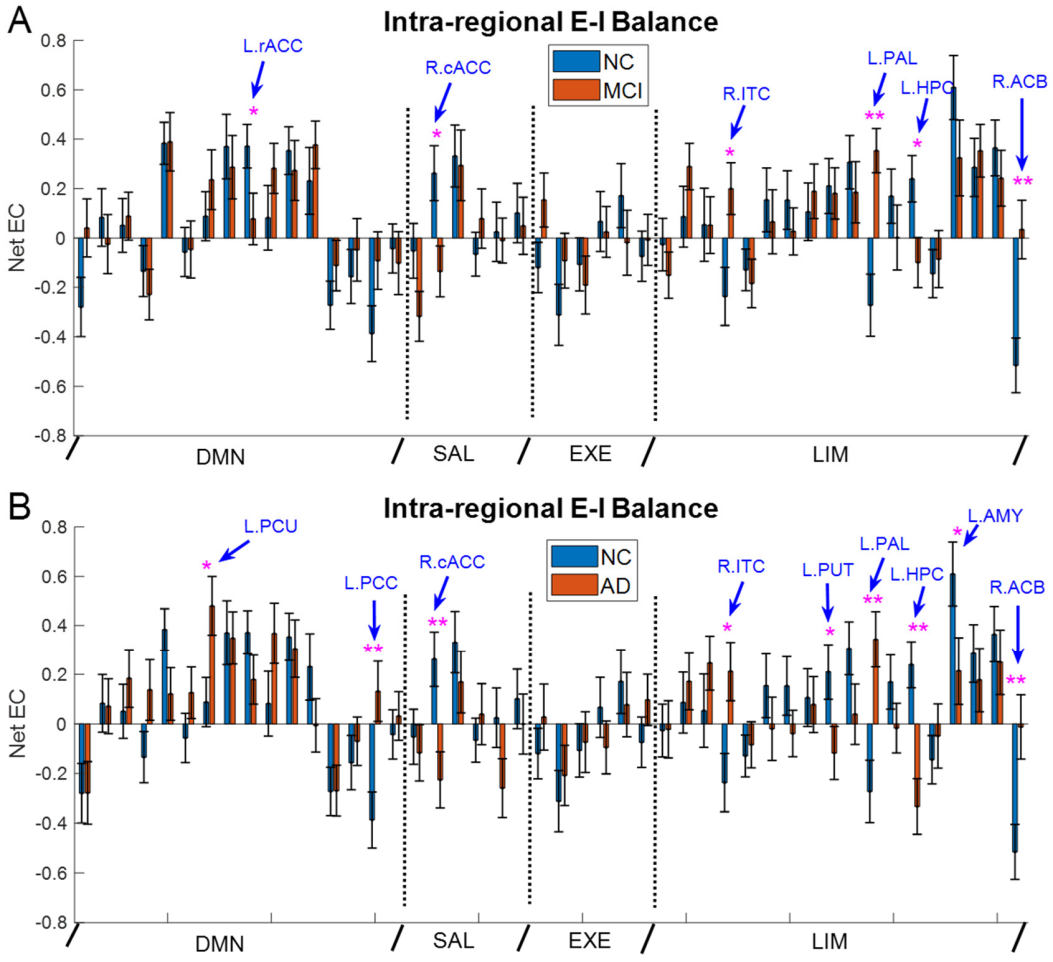

Figure 4. Disrupted intra-regional E-I balance in MCI and AD. (A) Net local EC in MCI. **(B)** Net local EC in AD. One star indicates uncorrected significance and double stars indicate corrected significance by FDR.

We next examined network-averaged recurrent excitation and inhibition change in MCI and AD. There was no significant difference between NC and MCI for average recurrent excitation (Fig. 5A1) while the executive control network showed decreased recurrent inhibition in MCI compared to NC ($p < 0.05$, uncorrected). By comparison, significant reduction in both recurrent excitation and recurrent inhibition was observed in the executive control network in AD and the change in recurrent inhibition survived multiple correction (Fig. 5B1, B2). Moreover, the default mode network also exhibited reduction in recurrent inhibition while the salience network showed increase in recurrent inhibition ($p < 0.05$, uncorrected; Fig. 5B2). Thus, on the network level, impairments in recurrent excitation and inhibition progressively increase from MCI to AD and the executive control network showed the most significant and consistent alterations. Again, the decrease in both recurrent excitation and inhibition may compensate the loss of each other, thus maintaining relatively stable E-I balance in the executive control network.

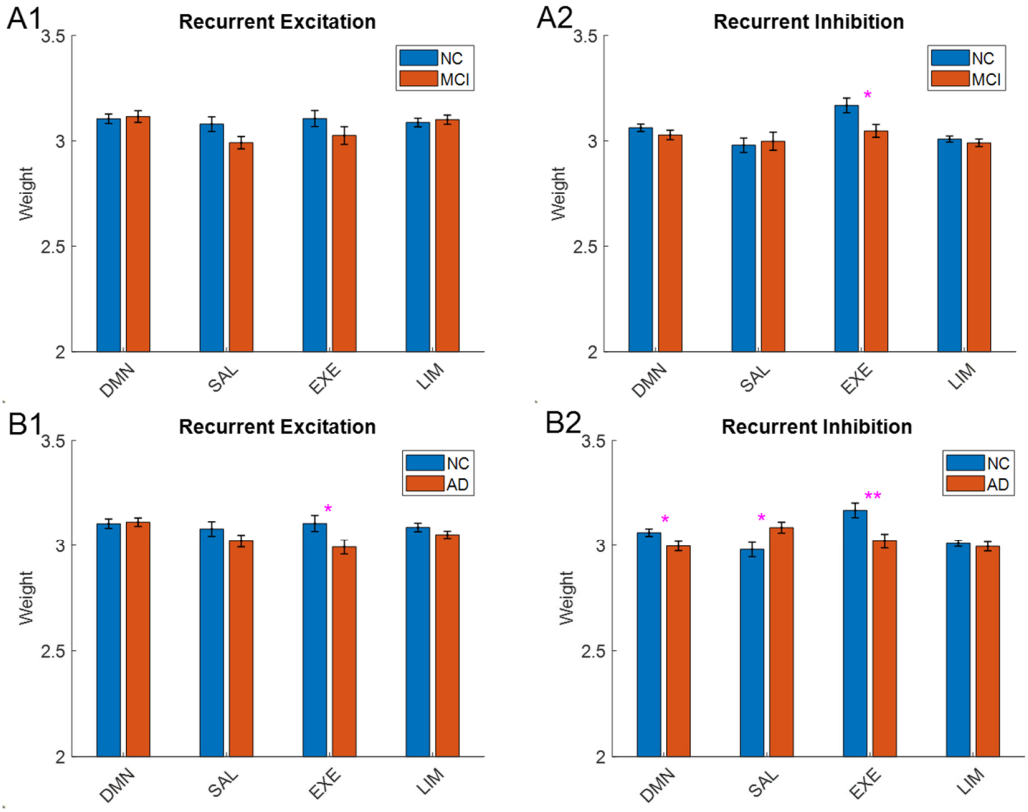

Figure 5. Network-averaged recurrent excitation and inhibition. (A1) Average recurrent excitation within four functional networks for NC and MCI. **(A2)** Average recurrent inhibition within four functional networks for NC and MCI. **(B1)** Average recurrent excitation within four functional networks for NC and AD. **(B2)** Average recurrent inhibition within four functional networks for NC and AD.

Disrupted inter-regional E-I balance in MCI and AD

In addition to intra-regional recurrent connections, inter-regional excitatory and inhibitory connections were also disrupted in MCI and AD. The color-coded average inter-regional EC matrices for NC, MCI and AD are shown in Fig. 6A, B, and C, respectively (the wide light blue area indicates the removed weaker connections). We observed that the EC patterns were similar for NC, MCI and AD where there were more excitatory (positive) connections than inhibitory (negative) connections. The significant EC connections in MCI (compared to NC) are indicated by the blue edges in Fig. 6D ($p < 0.05$, uncorrected), where they were distributed quite dispersedly among the four networks. The significant EC connections in AD (compared to NC) are shown in Fig. 6E where the blue edges indicated uncorrected significant connections and the red edges denoted significant connections that were corrected by NBS. Compared with MCI, the significant connections in AD concentrated more within and between the DMN and limbic networks. Of note, the corrected significant connections (red edges) involved mostly the executive control and limbic networks. Also, the average inter-regional EC of MCI was highly correlated with that of AD ($R = 0.6$, $p < 0.0001$; Fig. 6F), indicating the similar EC pattern between MCI and AD. To visualize the EC changes better, we compared the significant inter-regional EC between NC and MCI in Fig. 7A, and between NC and AD in Fig. 7B. As indicated by the EC difference in the bottom panels, most of the connections had less excitatory influence (or more inhibitory influence) in MCI and AD, indicating less excitatory communication between regions in MCI and AD. The corrected significant connections in AD included R.SPC→R.PUT, R.CA→R.THAL, R.SFC→R.PAL, R.PAL→R.PUT, R.rMFC→R.PUT, R.CA→R.rMFC, and R.PUT→R.PAL.

To evaluate the inter-reginal E-I balance change in MCI and AD, we computed the net inter-regional EC which is the summation of all incoming inter-regional EC to a particular ROI (Fig. 8). The net EC change from NC to MCI is shown in Fig. 8A where six regions showed impaired inter-regional E-I balance ($p < 0.05$, uncorrected). A majority of the six ROIs showed decreased net EC or excitation,

including L.PCU, R.IN, R.ITC, R.PUT and R.PAL, and only one ROI (R.cMFC) exhibited increased net EC. In AD, three common regions showed reduced net excitation as MCI, including R.ITC, R.PUT and R.PAL, all belonging to the limbic network (Fig. 8B). In particular, the significant changes in R.PUT and R.PAL were able to survive multiple correction by FDR, again indicating more severe E-I disruption in AD than MCI. Moreover, the net EC of L.HPC was also significantly reduced ($p < 0.05$), while the net EC of R.PCC was significantly elevated in AD ($p < 0.05$), both without passing multiple correction. On the network level, we observed the average net EC (summation of all excitatory and inhibitory inter-regional EC) from the executive network to the salience network was significantly decreased in MCI ($p < 0.05$, uncorrected; Fig. 9A, B). In AD, the average net EC from the executive network to the limbic network and from the DMN to the limbic network was also significantly reduced with the latter passing multiple correction (Fig. 9A, C), suggesting cortical-limbic decoupling. Overall, the excitatory influence between networks is substantially decreased in MCI and AD.

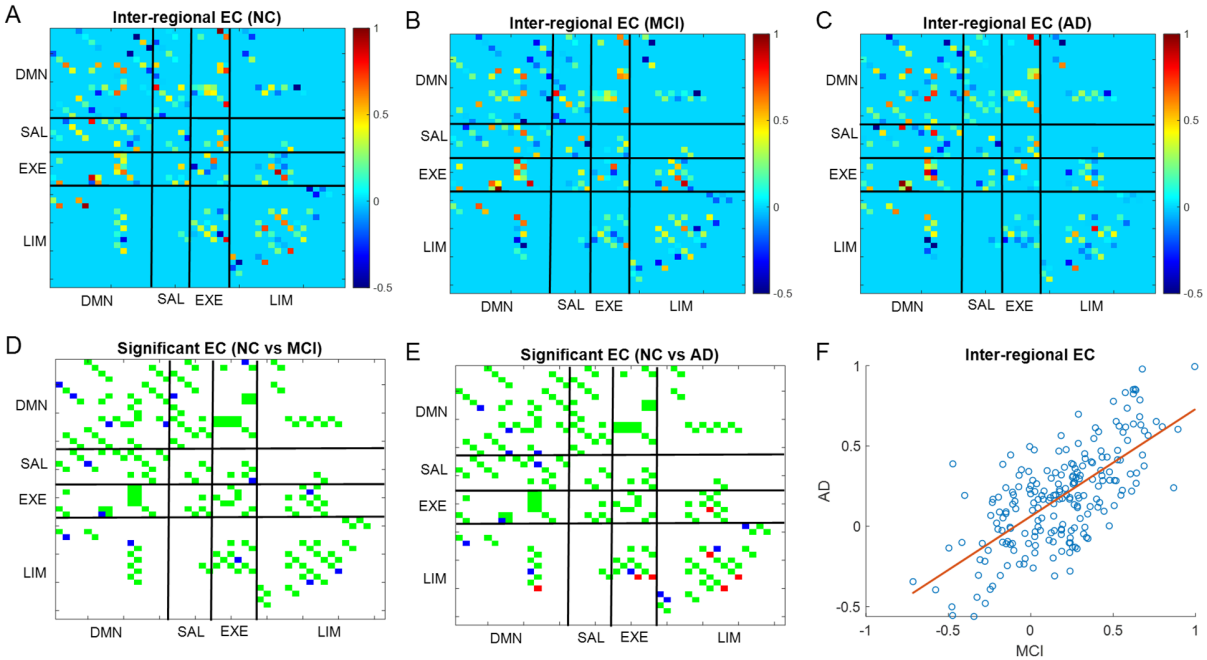

Figure 6. Inter-regional effective connectivity (EC) and significant EC connections. (A) Average inter-regional EC matrix for NC. **(B)** Average inter-regional EC matrix for MCI. **(C)** Average inter-regional EC matrix for AD. **(D)** Significant EC connections in MCI. **(E)** Significant EC connections in AD. **(F)** Correlation between average MCI inter-regional EC and average AD inter-regional EC. For **(D)** and **(E)**, green edges indicate insignificant nodes, blue edges indicate uncorrected significant nodes ($p < 0.05$), and red edges indicate significant nodes corrected by Network-based Statistics (NBS; $p < 0.05$).

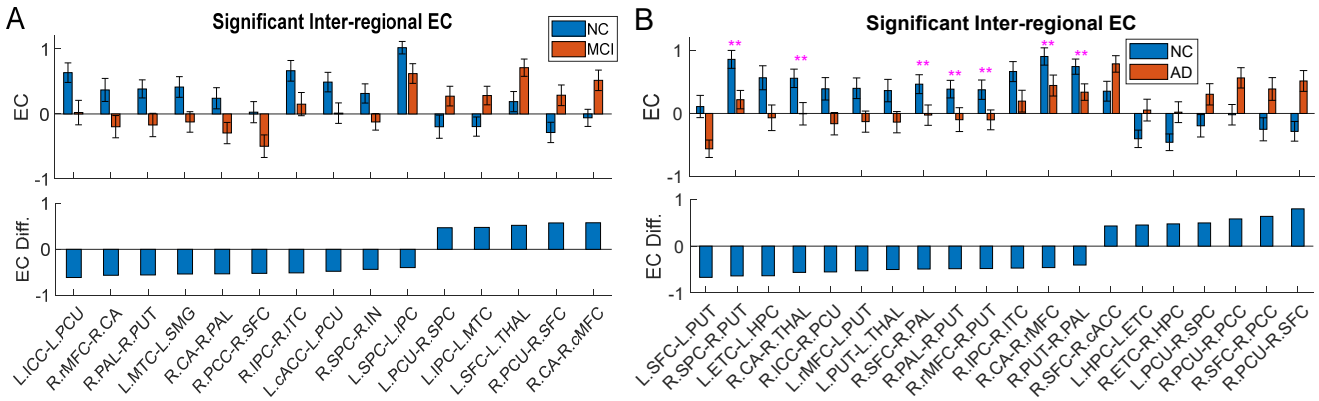

Figure 7. Comparison of significant inter-regional EC between NC and MCI (A) and between NC and AD (B). For both (A) and (B), the top panel plots the average inter-regional EC while the bottom panel plots the EC difference (i.e., change from NC to MCI or AD).

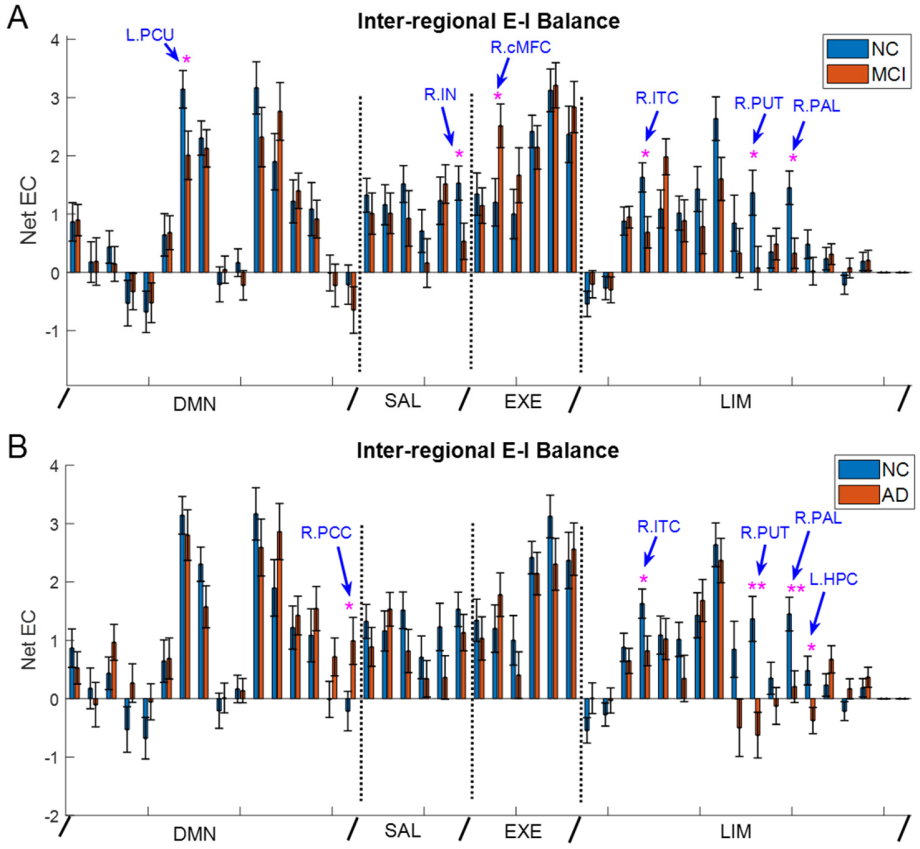

Figure 8. Disrupted inter-regional E-I balance in MCI and AD. (A) Net inter-regional EC in MCI. **(B)** Net inter-reginal EC in AD.

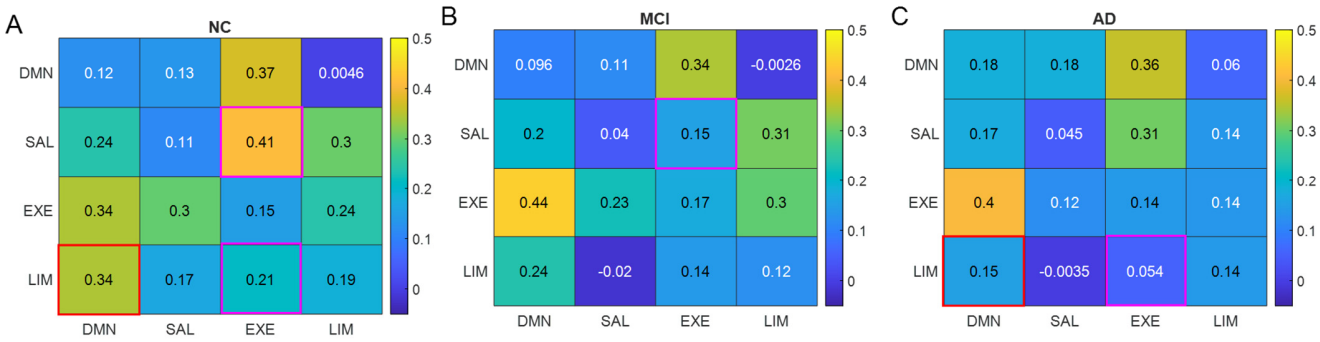

Figure 9. Altered inter-network connection strength in MCI and AD. (A) Average inter-network EC in NC. **(B)** Average inter-network EC in MCI. **(C)** Average inter-network EC in AD. Pink box indicates uncorrected significance ($p < 0.05$) and red box indicates corrected significance ($p < 0.05$).

Disrupted overall E-I balance in MCI and AD

The above analysis indicates that both intra-regional and inter-regional E-I balance are impaired in MCI and AD. As the overall neural excitability depends on both intra-regional and inter-regional input drive, we computed the overall E-I balance as the ratio of net excitation (recurrent excitation + all incoming excitatory inter-regional EC) to net inhibition (recurrent inhibition + all incoming inhibitory inter-regional EC) for all ROIs. We found that the overall E-I balance was altered in a number of regions in MCI and AD and most of the regions were located in the limbic network (Fig. 10). Specifically, the E-I ratio of R.IN, R.PUT, R.PAL and L.HPC was significantly decreased ($p < 0.05$), while that of R.cMFC and R.ACB was significantly increased in MCI ($p < 0.05$); the change in R.PAL and R.ACB survived multiple correction (Fig. 10A). Notably, in both MCI and AD, the changes in overall E-I balance remained consistent for R.PUT, R.PAL, L.HPC and R.ACB, all four regions from the limbic network (compare Fig. 10B with 10A). In addition to R.PAL and R.ACB, the E-I balance changes in R.PUT and L.HPC were able to pass multiple correction in AD. Besides, the overall E-I ratio of L.IN and L.PUT was significantly reduced, while that of L.PCC, R.PCC, L.ETC and R.HPC was significantly increased in AD, all without surviving multiple correction. Overall, the majority of disrupted regions show reduced E-I ratio and the alteration of E-I balance is the most stable in the limbic network during AD progression. Lastly, we examined the change of spontaneous input during AD progression. There was no difference in

spontaneous input between NC and MCI, while the spontaneous input was significantly decreased in AD ($p < 0.05$; Fig. 11). This suggests that the overall excitatory drive to the network is reduced in the AD phase, consistent with overall reduction in E-I balance.

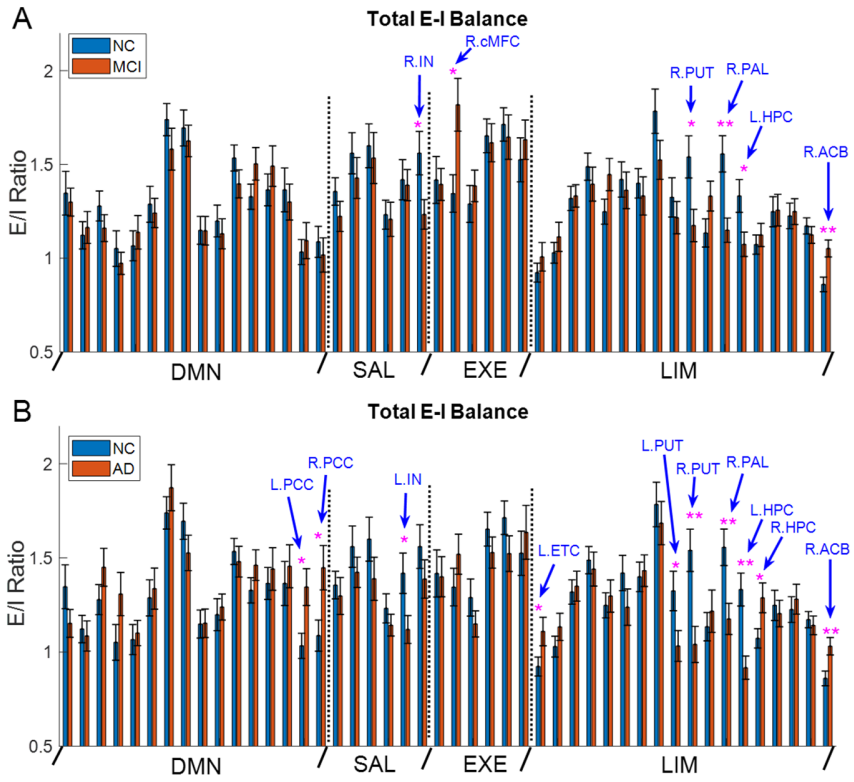

Figure 10. Impaired overall E-I balance in MCI and AD. (A) Comparison of overall E-I balance between NC and MCI. **(B)** Comparison of overall E-I balance between NC and AD.

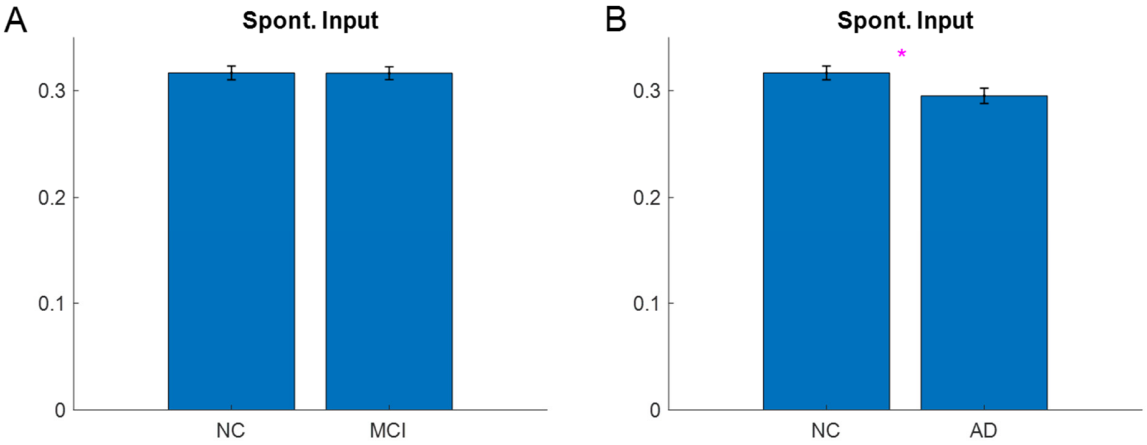

Figure 11. Evolution of spontaneous input during AD progression. (A) Comparison of spontaneous input between NC and MCI. **(B)** Comparison of spontaneous input between NC and AD.

Discussion

Excitation-inhibition (E-I) balance is a fundamental property of neuronal circuits that regulates multiple essential brain functions such as information coding, synaptic plasticity, memory stability and neurogenesis (Deneve and Machens, 2016; Rubin et al., 2017; Bhatia et al., 2019; Lopatina et al., 2019; Sadeh and Clopath, 2021). Disruption of E-I balance has been implicated in both AD animal models (Palop et al., 2007; Verret et al., 2012) and human AD (Dickerson et al., 2004, 2005; Celone et al., 2006; Bakker et al., 2012). Converging evidence suggests that E-I imbalance is a critical regulator of AD pathology (Palop and Mucke, 2010; Busche and Konnerth, 2016; Palop and Mucke, 2016; Frere and Slutsky, 2018; Styr and Slutsky, 2018; Ambrad et al., 2019) and may represent a core element that underpins a "central feature" of AD linking multi-levels of analysis (Maestú et al., 2021). Identifying pathological E-I balance during the progression of AD thus constitutes an important first step to develop new diagnostic techniques that use E-I imbalance as a biomarker and new treatment paradigms that aim to restore E-I imbalance for early intervention. However, current analytical approaches in fMRI focus predominantly on statistical techniques and macroscopic modeling such as static/dynamic functional connectivity, independent component analysis and graph theory (Sporns, 2014; Li et al., 2009; Preti et al., 2017), which cannot identify disrupted E-I balance at cellular and circuit levels. Using a recently developed Multiscale Neural Model Inversion (MNMI) framework, we identified disrupted E-I balance along with impaired excitatory and inhibitory neural interactions in a large network during AD progression. Our study provides both a novel framework to measure pathological E-I balance and important insights into the systematic features and circuit mechanisms of E-I alterations.

Systematic features of E-I alterations

One important hallmark of AD pathology is the progressive disruption of synaptic transmission (Sheng et al., 2012; Marsh and Alifragis, 2018). Consistently, we demonstrated that both excitatory and inhibitory interactions are substantially altered during the progress of AD and such alterations exhibit systematic

features. First, excitatory and inhibitory connections are progressively disrupted during AD progression. For both intra-regional and inter-regional neural interactions, more connections are impaired in AD than MCI and the degree of impairments also becomes more significant in AD. This suggests that E-I imbalance parallels AD development and is causally linked to AD pathology. Second, AD pathology differentially alters excitatory and inhibitory connections. Compared with recurrent excitatory connections, more recurrent inhibitory connections are impaired and to a greater extent, in agreement with the emerging viewpoint of GABAergic dysfunction in AD (Li et al., 2016; Palop and Mucke, 2016; Xu et al., 2020). Importantly, alterations of inhibitory connections exhibit a more stable pattern than excitatory connections as consistent impairments are observed across MCI and AD (Fig. 3). Lastly, AD progression is associated with a general decoupling of excitatory and inhibitory interactions. Although the strength of excitatory and inhibitory connections could either increase of decrease in MCI/AD, reduction of connection strengths dominates increasing ones for both intra-regional and inter-regional connections (Fig. 3 and Fig. 7), consistent with the "synaptic dismantling" theory of AD (Selkoe et al., 2002). The heterogenous but reduction-dominated alterations in excitatory/inhibitory coupling strengths (i.e., effective connectivity) also concord with the observed bidirectional change yet widespread decrease in functional connectivity in MCI and AD (Filippi and Agosta, 2011; Brier et al., 2014; Dennis and Thompson, 2014).

Bidirectional alteration of E-I balance

One important finding of this study is that we observed bidirectional alteration of E-I balance. Depending on the specific modulation of excitatory and inhibitory connections, E-I balance can be either increase or decrease for different regions. Our findings are consistent with experimental data that hyperactive neurons coexist with hypoactive neurons in AD mouse model (Busche et al., 2008) and MCI and AD are associated with both regional hyperactivation and hypoactivation in human (Celon et al., 2006; Corriveau-Lecavalier et al., 2019). We further reveal that increase of E-I balance is mostly due to decease of

inhibitory connections (Fig. 3 and Fig. 4), in agreement with experimental findings that neuronal hyperactivity is a result of decreased synaptic inhibition (Busche et al., 2008). Of note, studies have revealed alteration of E-I balance depends on the stage of AD progression where the HPC shows hyperactivity in aMCI, but reduced activities in late aMCI and AD (Dickerson et al., 2004, 2005; Celone et al., 2006). By comparison, modeling results indicate that alterations in E-I balance remain consistent across MCI and AD for the same region and HCP exhibits reduced E-I balance throughout (Figs. 3, 4, 10). This may be due to the fact that elevated E-I balance in HPC is a temporal event in the early aMCI stage, similar to the transient increase of FC in the DMN and salience networks at the very mild AD phase (Brier et al., 2012), while MCI patients included in this study are already in the moderate or late MCI phase.

A core network of E-I imbalance in AD

Despite the heterogeneous and distributed changes in E-I interactions, we observed stable patterns of E-I disruptions in a set of brain regions including the HPC, pallidum, putamen, nucleus accumbens, inferior temporal cortex (ITC) and caudal anterior cingulate cortex (cACC). These brain regions are consistently impaired across MCI and AD for intra-reginal E-I balance (Fig. 3), inter-regional E-I balance (Fig. 8) or overall E-I balance (Fig. 10). Such a core network highlights the paramount importance of the limbic/subcortical regions and cingulate areas in AD pathophysiology. The involvement of HPC, the core region in the memory network, is consistent with the vast majority of literatures about the central role of this critical structure in AD (Dickerson et al., 2004, 2005; Wang et al., 2006; Palop et al., 2007; Bakker et al., 2012). The reduction of E-I balance in HPC due to increased inhibition is also consistent with the experimental findings that high GABA content in reactive astrocytes of the dentate gyrus was discovered in brain samples from human AD patients as well as AD mouse model resulting in increased tonic inhibition and memory deficit (Wu et al., 2014). The stable participation of the basal ganglia including pallidum, putamen and nucleus accumbens in E-I disruption is somewhat unexpected as the primary function of this subcortical structure is motor control (Groenewegen, 2003), but not completely surprising

because recent studies have revealed the disturbance of basal ganglia in dementia traditionally classified as motor disorders (Vitanova et al., 2019). Specifically, MRI studies have consistently revealed substantial volume reduction in the basal ganglia including the putamen and caudate nucleus (Cho et al., 2014; de Jong et al., 2008, 2011). The striatum, consisting of the putamen, nucleus accumbens and caudate nucleus, is particularly susceptible to AD degeneration since both Aβ plaques and neurofibrillary tangles (NFT) of hyperphosphorylated tau are found in the stratal regions (Vitanova et al., 2019) and Aβ deposition starts in the striatum of presenilin-1 mutation carriers (Klunk et al., 2007). Importantly, Aβ may even begin to develop in the striatum 10 years before expected symptom onset (Bateman et al., 2012), suggesting that the basal ganglia could be an important pathophysiological target in AD that is affected early in the Aβ cascade but has not yet receive sufficient investigation. Because the basal ganglia are thought to contribute to cognitive function (Leisman et al., 2014), disruption of its nuclei would lead to cognitive and memory impairments in AD. The ITC plays an important role in verbal fluency, a cognitive function that is compromised during the early AD onset stage (Bouras et al., 1994). The disruption of E-I balance in ITC is consistent with the significant synaptic loss in this region in individuals with aMCI (Scheff et al., 2011), which may underlie early AD symptomatology. Lastly, the anterior cingulate cortex (ACC) plays a vital role in multiple cognitive process including executive function, memory and emotion (Carter et al., 1999; Bush et al., 2000; Weible et al., 2013). It is one of the earliest affected areas by Aβ accumulation (Braak et al., 1991; Raj et al., 2012) and exhibits disrupted FC in MCI and AD (Liang et al., 2015; Liu et al., 2017). It has been demonstrated that Aβ altered E-I balance in ACC through inhibiting presynaptic GABA-release from fast-spiking interneurons onto pyramidal cells (Ren et al., 2018). Overall, with consistent and significant E-I disruption, the core network may represent a stable biomarker and an important therapeutic target in AD.

Conclusions

Using a multiscale neural model inversion framework, we identified disrupted E-I balance as well as impaired excitatory and inhibitory connections during AD progression. We observed that E-I balance is progressively disrupted from MCI to AD and alteration of E-I balance is bidirectional varying from region to region. Also, we found that inhibitory connections are more significantly impaired than excitatory connections and the strength of the majority of excitatory and inhibitory connections reduces in MCI and AD, leading to gradual decoupling of neural populations. Moreover, we revealed a core AD network comprising mainly of limbic and cingulate regions exhibit consistent and stable E-I alteration across MCI and AD, which may represent an important therapeutic target to restore pathological E-I balance.

References

Abeysuriya RG, Hadida J, Sotiropoulos SN, Jbabdi S, Becker R, Hunt BAE, et al. (2018) A biophysical model of dynamic balancing of excitation and inhibition in fast oscillatory large-scale networks. *PLoS Comput Biol* 14: e1006007.

Aldehri M, Temel Y, Alnaami I, Jahanshahi A, Hescham S (2018) Deep brain stimulation for Alzheimer's disease: an update. *Surg Neurol Int* 9: 58.

Allen G, Barnard H, McColl R, Hester AL, Fields JA,Weiner MF, Ringe WK, Lipton AM, Brooker M, McDonald E, Rubin CD, Cullum CM (2007) Reduced hippocampal functional connectivity in Alzheimer disease. *Arch Neurol* 64: 1482-1487.

Alzheimer's Association (2016) 2016 Alzheimer's disease facts and figures. *Alzheimer's Dement* 12: 459–509.

Ambrad Giovannetti E, Fuhrmann M (2019) Unsupervised excitation: GABAergic dysfunctions in Alzheimer's disease. *Brain Res* 1707: 216–226.

Bai F, Watson DR, Yu H, Shi Y, Yuan Y, Zhang Z (2009) Abnormal resting-state functional connectivity of posterior cingulate cortex in amnestic type mild cognitive impairment. *Brain Res* 1302: 167-174.

Bakker A, Krauss GL, Albert MS, Speck CL, Jones LR, Stark CE, Yassa MA, Bassett SS, Shelton AL, Gallagher M (2012) Reduction of hippocampal hyperactivity improves cognition in amnestic mild cognitive impairment. *Neuron* 74: 467–474.

Bateman RJ, Xiong C, Benzinger TL, Fagan AM, Goate A, Fox NC, Marcus DS, Cairns NJ, Xie X, Blazey TM, Holtzman DM, Santacruz A, Buckles V, Oliver A, Moulder K, Aisen PS, Ghetti B, Klunk WE, McDade E, Martins RN, Masters CL, Mayeux R, Ringman JM, Rossor MN, Schofield PR, Sperling RA, Salloway S, Morris JC (2012) Dominantly Inherited Alzheimer Network. Clinical and biomarker changes in dominantly inherited Alzheimer's disease. *N Engl J Med* 367: 795-804.

Becker R, Knock S, Ritter P, Jirsa V (2015) Relating alpha power and phase to population firing and hemodynamic activity using a thalamo-cortical neural mass model. *PLoS Comput Biol* 11: e1004352.

Bero AW, Yan P, Roh JH, Cirrito JR, Stewart FR, Raichle ME, Lee JM, Holtzman DM (2011) Neuronal activity regulates the regional vulnerability to amyloid-β deposition. *Nat Neurosci* 14: 750–756.

Bhatia A, Moza S, Bhalla US (2019) Precise excitation-inhibition balance controls gain and timing in the hippocampus. *Elife* 8: e43415.

Bouras C, Hof PR, Giannakopoulos P, Michel JP, Morrison JH (1994) Regional distribution of neurofibrillary tangles and senile plaques in the cerebral cortex of elderly patients: a quantitative evaluation of a one-year autopsy population from a geriatric hospital. *Cereb Cortex* 4: 138–150.

Braak H, Braak E (1991) Neuropathological stageing of Alzheimer-related changes. *Acta Neuropathol* 82: 239–259.

Brier MR, Thomas JB, Ances BM (2014) Network dysfunction in Alzheimer's disease: refining the disconnection hypothesis. *Brain Connect* 4: 299-311.

Brier MR, Thomas JB, Snyder AZ, Benzinger TL, Zhang D, Raichle ME, Holtzman DM, Morris JC, Ances BM (2012) Loss of intranetwork and internetwork resting state functional connections with Alzheimer's disease progression. *J Neurosci* 32: 8890–8899.

Busche MA, Eichhoff G, Adelsberger H, Abramowski D, Wiederhold KH, Haass C, Staufenbiel M, Konnerth A, Garaschuk O (2008) Clusters of hyperactive neurons near amyloid plaques in a mouse model of Alzheimer's disease. *Science* 321: 1686–1689.

Busche MA, Kekus M, Adelsberger H, Noda T, Forstl H, Nelken I, Konnerth A (2015) Rescue of long range circuit dysfunction in Alzheimer's disease models. *Nat Neurosci* 18: 1623–1630.

Busche MA, Konnerth A (2016) Impairments of neural circuit function in Alzheimer's disease. *Philos Trans R Soc Lon B Biol Sci* 371: 20150429.

Bush G, Luu P, Posner MI (2000) Cognitive and emotional influences in anterior cingulate cortex. *Trends Cogn Sci* 4: 215–222.

Carter CS, Botvinick MM, Cohen JD (1999) The contribution of the anterior cingulate cortex to executive processes in cognition. *Rev Neurosci* 10: 49–57.

Celone KA, Calhoun VD, Dickerson BC, Atri A, Chua EF, Miller SL, DePeau K, Rentz DM, Selkoe DJ, Blacker D, et al. (2006) Alterations in memory networks in mild cognitive impairment and Alzheimer's disease: an independent component analysis. *J Neurosci* 26: 10222–10231.

Cho H, Kim J-H, Kim C, Ye BS, Kim HJ, Yoon CW, Seo SW (2014) Shape changes of the basal ganglia and thalamus in Alzheimer's disease: A three-year longitudinal study. *Journal of Alzheimer's Disease* 40: 285–295.

Cohen AD, Price JC, Weissfeld LA, James J, Rosario BL, Bi W, Nebes RD, Saxton JA, Snitz BE, Aizenstein HA, Wolk DA, Dekosky ST, Mathis CA, Klunk WE (2009) Basal cerebral metabolism may modulate the cognitive effects of Aβ in mild cognitive impairment: an example of brain reserve. *J Neurosci* 29: 14770–14778.

Corriveau-Lecavalier N, Mellah S, Clément F, Belleville S (2019) Evidence of parietal hyperactivation in individuals with mild cognitive impairment who progressed to dementia: A longitudinal fMRI study. *Neuroimage Clin* 24: 101958.

Cox RW, Hyde JS (1997) Software tools for analysis and visualization of fMRI data. *NMR Biomed* 10: 171–178.

de Haan W, Mott K, van Straaten EC, Scheltens P, Stam CJ (2012) Activity dependent degeneration explains hub vulnerability in Alzheimer's disease. *PLoS Comput Biol* 8: e1002582.

de Haan, W, van Straaten ECW, Gouw AA, Stam CJ (2017) Altering neuronal excitability to preserve network connectivity in a computational model of Alzheimer's disease. *PLoS Comput Biol* 13: e1005707.

de Jong LW, Ferrarini L, van der Grond J, Milles JR, Reiber JHC, Westendorp RGJ, … van Buchem MA (2011) Shape abnormalities of the striatum in Alzheimer's disease. *Journal of Alzheimer's Disease* 23: 49–59.

de Jong LW, van der Hiele K, Veer IM, Houwing JJ, Westendorp RGJ, Bollen ELEM, … van der Grond J (2008) Strongly reduced volumes of putamen and thalamus in Alzheimer's disease: An MRI study. *Brain* 131: 3277–3285.

Deco G, Ponce-Alvarez A, Mantini D, Romani GL, Hagmann P, Corbetta M (2013) Resting-state functional connectivity emerges from structurally and dynamically shaped slow linear fluctuations. J Neurosci 33: 11239–11252.

Delbeuck, X., Van der Linden, M., Collette, F., 2003. Alzheimer's disease as a disconnection syndrome? Neuropsychol. Rev. 13, 79–92.

Deneve S, Machens CK (2016) Efficient codes and balanced networks. *Nat Neurosci* 19: 375–382.

Dennis EL, Thompson PM (2014) Functional brain connectivity using fMRI in aging and Alzheimer's disease. *Neuropsychol Rev* 24: 49-62.

Desikan RS, Ségonne F, Fischl B, Quinn BT, Dickerson BC, Blacker D, Buckner RL, Dale AM, Maguire RP, Hyman BT, Albert MS, Killiany RJ (2006) An automated labeling system for subdividing the human cerebral cortex on MRI scans into gyral based regions of interest. *Neuroimage* 31: 968–980.

Dickerson BC, Salat DH, Bates JF, Atiya M, Killiany RJ, Greve DN, Dale AM, Stern CE, Blacker D, Albert MS, Sperling RA (2004) Medial temporal lobe function and structure in mild cognitive impairment. *Ann Neurol* 56: 27–35.

Dickerson BC, Salat DH, Greve DN, Chua EF, Rand-Giovannetti E, Rentz DM, Bertram L, Mullin K, Tanzi RE, Blacker D, et al. (2005) Increased hippocampal activation in mild cognitive impairment compared to normal aging and AD. *Neurology* 65: 404–411.

Filippi M, Agosta F (2011) Structural and functional network connectivity breakdown in Alzheimer's disease studied with magnetic resonance imaging techniques. *J Alzheimers Dis* 24: 455-474.

Fox MD, Raichle ME (2007) Spontaneous fluctuations in brain activity observed with functional magnetic resonance imaging. *Nature Reviews Neuroscience* 8: 700–711.

Frässle S, Lomakina EI, Razi A, Friston KJ, Buhmann JM, Stephan KE (2017) Regression DCM for fMRI. *Neuroimage* 155: 406–421.

Frere S, Slutsky I (2018) Alzheimer's disease: from firing instability to homeostasis network collapse. *Neuron* 97: 32–58.

Friston K, Fletcher P, Josephs O, Holmes A, Rugg M, Turner R (1998) Event-related fMRI: characterizing differential responses. *Neuroimage* 7: 30–40.

Glover GH (2011). Overview of functional magnetic resonance imaging. *Neurosurg Clin N Am* 22: 133-139.

Greicius MD, Srivastava G, Reiss AL, Menon V (2004) Default-mode network activity distinguishes Alzheimer's disease from healthy aging: evidence from functional MRI. *Proc Natl Acad Sci USA* 101: 4637–4642.

Groenewegen HJ (2003) The basal ganglia and motor control. *Neural Plast* 10: 107-120.

Hellyer PJ, Jachs B, Clopath C, Leech R (2016) Local inhibitory plasticity tunes macroscopic brain dynamics and allows the emergence of functional brain networks. *Neuroimage* 124: 85–95.

Huang Y, Mucke L (2012) Alzheimer mechanisms and therapeutic strategies. *Cell* 148: 1204–1222.

Hughes SW, Crunelli V (2005) Thalamic mechanisms of EEG alpha rhythms and their pathological implications. *Neuroscientist* 11: 357-372.

Jack CR Jr, Bernstein MA, Fox NC, Thompson P, Alexander G, Harvey D, Borowski B, Britson PJ, L Whitwell J, Ward C, Dale AM, Felmlee JP, Gunter JL, Hill DL, Killiany R, Schuff N, Fox-Bosetti S, Lin C, Studholme C, DeCarli CS, Krueger G, Ward HA, Metzger GJ, Scott KT, Mallozzi R, Blezek D, Levy J, Debbins JP, Fleisher AS, Albert M, Green R, Bartzokis G, Glover G, Mugler J, Weiner MW (2008) The Alzheimer's Disease Neuroimaging Initiative (ADNI): MRI methods. *J Magn Reson Imaging* 27: 685-691.

Johnson SC, Christian BT, Okonkwo OC, Oh JM, Harding S, Xu G, et al. (2014) Amyloid burden and neural function in people at risk for Alzheimer's disease. *Neurobiol Aging* 35: 576–584.

Karran E, Mercken M, De Strooper B (2011) The amyloid cascade hypothesis for Alzheimer's disease: an appraisal for the development of therapeutics. *Nat Rev Drug Discov* 10: 698–712.

Klunk WE, Price JC, Mathis CA, Tsopelas ND, Lopresti BJ, Ziolko SK, DeKosky ST (2007) Amyloid deposition begins in the striatum of presenilin-1 mutation carriers from two unrelated pedigrees. *Journal of Neuroscience* 27: 6174–6184.

Koechlin E, Summerfield C (2007) An information theoretical approach to prefrontal executive function. *Trends Cogn Sci* 1: 229-235.

Leisman G, Braun-Benjamin O, Melillo R (2014) Cognitive-motor interactions of the basal ganglia in development. *Front Syst Neurosci* 8: 16.

Li G, Liu Y, Zheng Y, Wu Y, Li D, Liang X, Chen Y, Cui Y, Yap P, Qiu S, Zhang H, Shen D (2021) Multiscale neural modeling of resting-state fMRI reveals executive-limbic malfunction as a core mechanism in major depressive disorder. *Neuroimage: Clinical* 31: 102758.

Li G, Yap P-T (2022) From descriptive connectome to mechanistic connectome: Generative modeling in functional magnetic resonance imaging analysis. *Front Hum Neurosci 16*: 940842.

Li K, Guo L, Nie J, Li G, Liu T (2009) Review of methods for functional brain connectivity detection using fMRI. *Comput Med Imaging Graph* 33: 131–139.

Li Y, Sun H, Chen Z, Xu H, Bu G and Zheng H (2016) Implications of GABAergic neurotransmission in Alzheimer's Disease. *Front Aging Neurosci* 8: 31.

Liang Y, Chen Y, Li H, Zhao T, Sun X, Shu N, Peng D, Zhang Z (2015) Disrupted functional connectivity related to differential degeneration of the cingulum bundle in mild cognitive impairment patients. *Curr Alzheimer Res* 12: 255-265.

Liu X, Chen W, Hou H, et al. (2017) Decreased functional connectivity between the dorsal anterior cingulate cortex and lingual gyrus in Alzheimer's disease patients with depression. *Behavioural Brain Research* 326: 132-138.

Lopatina OL, Malinovskaya NA, Komleva YK, Gorina YV, Shuvaev AN, Olovyannikova RY, Belozor OS, Belova OA, Higashida H, Salmina AB (2019) Excitation/inhibition imbalance and impaired neurogenesis in neurodevelopmental and neurodegenerative disorders. *Rev Neurosci* 30: 807–820.

Lustig C, Snyder AZ, Bhakta M, O'Brien KC, McAvoy M, Raichle ME, Morris JC, Buckner RL (2003) Functional deactivations: change with age and dementia of the Alzheimer type. *Proc Natl Acad Sci USA* 100: 14504–14509.

Maestú F, de Haan W, Busche MA, DeFelipe J (2021) Neuronal excitation/inhibition imbalance: core element of a translational perspective on Alzheimer pathophysiology. *Ageing Res Rev* 69: 101372.

Marsh J, Alifragis P (2018) Synaptic dysfunction in Alzheimer's disease: the effects of amyloid beta on synaptic vesicle dynamics as a novel target for therapeutic intervention. *Neural Regen Res* 13: 616-623.

Miller EK, Cohen JD (2001) An integrative theory of prefrontal cortex function. *Annu Rev Neurosci* 24: 167-202.

Mormino EC, Brandel MG, Madison CM, Marks S, Baker SL, Jagust WJ (2012) Aβ deposition in aging is associated with increases in brain activation during successful memory encoding. *Cereb Cortex* 22: 1813–1823.

Nitsch RM, Farber SA, Growdon JH, Wurtman RJ (1993) Release of amyloid beta- protein precursor derivatives by electrical depolarization of rat hippocampal slices. *Proc Natl Acad Sci USA* 90: 5191–5193.

Palop JJ, Chin J, Roberson ED, Wang J, Thwin MT, Bien-Ly N, Yoo J, Ho KO, Yu GQ, Kreitzer A, Finkbeiner S, Noebels JL, Mucke L (2007) Aberrant excitatory neuronal activity and compensatory remodeling of inhibitory hippocampal circuits in mouse models of Alzheimer's disease. *Neuron* 55: 697–711.

Palop JJ, Mucke L (2009) Epilepsy and cognitive impairments in Alzheimer's disease. *Archives of Neurology* 66: 435–440.

Palop JJ, Mucke L (2010) Amyloid-β-induced neuronal dysfunction in Alzheimer's disease: from synapses toward neural networks. *Nat Neurosci* 13: 812–818.

Palop J, Mucke L (2016) Network abnormalities and interneuron dysfunction in Alzheimer's disease. *Nat Rev Neurosci* 17: 777–792.

Petrides M (2005) Lateral prefrontal cortex: architectonic and functional organization. *Philos Trans R Soc Lond B: Biol Sci* 360: 781-795.

Pihlajamäki M, Sperling RA (2009) Functional MRI assessment of task-induced deactivation of the default mode network in Alzheimer's disease and at-risk older individuals. *Behav Neurol* 21: 77–91.

Power JD, Barnes KA, Snyder AZ, Schlaggar BL, Petersen SE (2012) Spurious but systematic correlations in functional connectivity MRI networks arise from subject motion. *Neuroimage* 59: 2142–2154.

Preti MG, Bolton TA, Van De Ville D (2017) The dynamic functional connectome: State-of-the-art and perspectives. *Neuroimage* 160: 41–54.

Qi Z, Wu X, Wang Z, Zhang N, Dong H, Yao L, Li K (2010) Impairment and compensation coexist in amnestic MCI default mode network. *Neuroimage* 50, 48-55.

Raichle ME, MacLeod AM, Snyder AZ, Powers WJ, Gusnard DA, Shulman GL (2001) A default mode of brain function. *Proc Natl Acad Sci USA* 98: 676-682.

Raj A, Kuceyeski A, Weiner M (2012) A network diffusion model of disease progression in dementia. *Neuron* 73: 1204–1215.

Ren SQ, Yao W, Yan JZ, Jin C, Yin JJ, Yuan J, Yu S, Cheng Z (2018) Amyloid β causes excitation/inhibition imbalance through dopamine receptor 1-dependent disruption of fast-spiking GABAergic input in anterior cingulate cortex. *Sci Rep* 8: 302.

Rombouts SA, Barkhof F, Goekoop R, Stam CJ, Scheltens P (2005) Altered resting state networks in mild cognitive impairment and mild Alzheimer's disease: an fMRI study. *Hum Brain Mapp* 26: 231–239.

Rubin R, Abbott LF, Sompolinsky H (2017) Balanced excitation and inhibition are required for high-capacity, noise-robust neuronal selectivity. *Proc Natl Acad Sci USA* 114: E9366–E9375.

Sadeh S, Clopath C (2021) Excitatory-inhibitory balance modulates the formation and dynamics of neuronal assemblies in cortical networks. *Sci Adv* 7: eabg8411.

Sanz-Arigita EJ, Schoonheim MM, Damoiseaux JS, Rombouts SA, Maris E, Barkhof F, Scheltens P, Stam CJ (2010) Loss of 'small-world' networks in Alzheimer's disease: graph analysis of FMRI resting-state functional connectivity. *PLoS One* 5: e13788.

Scheff SW, Price DA, Schmitt FA, Scheff MA, Mufson EJ (2011) Synaptic loss in the inferior temporal gyrus in mild cognitive impairment and Alzheimer's disease. *J Alzheimers Dis* 24: 547-557.

Selkoe DJ (2002) Alzheimer's disease is a synaptic failure. *Science* 298: 789–791.

Sheng M, Sabatini BL, Südhof TC (2012) Synapses and Alzheimer's disease. *Cold Spring Harb Perspect Biol* 4: a005777.

Sorg C, Riedl V, Muhlau M, Calhoun VD, Eichele T, Laer L, Drzezga A, Forstl H, Kurz A, Zimmer C, Wohlschlager AM (2007) Selective changes of resting-state networks in individuals at risk for Alzheimer's disease. *Proc Natl Acad Sci USA* 104: 18760-18765.

Sporns O (2014) Contributions and challenges for network models in cognitive neuroscience. *Nat Neurosci* 17: 652–660.

Stam CJ, Jones BF, Nolte G, Breakspear M, Scheltens P (2007) Small-world networks and functional connectivity in Alzheimer's disease. Cereb Cortex 17: 92–99.

Styr B, Slutsky I (2018) Imbalance between firing homeostasis and synaptic plasticity drives early-phase Alzheimer's disease. *Nat Neurosci* 21: 463–473.

Supekar K, Menon V, Rubin D, Musen M, Greicius MD (2008) Network analysis of intrinsic functional brain connectivity in Alzheimer's disease. *PLoS Comput Biol* 4: e1000100.

Thakur AK, Kamboj P, Goswami K (2018) Pathophysiology and management of Alzheimer's disease: an overview. *J Anal Pharm Res* 9: 226–235.

Tiwari S, Atluri V, Kaushik A, Yndart A, Nair M (2019) Alzheimer's disease: pathogenesis, diagnostics, and therapeutics. *Int J Nanomedicine* 14: 5541–5554.

Tong Y, Hocke LM, Frederick BB (2019) Low frequency systemic hemodynamic "noise" in resting state BOLD fMRI: characteristics, causes, implications, mitigation strategies, and applications. *Front Neurosci* 13: 787.

Van Essen DC, Smith SM, Barch DM, Behrens TEJ, Yacoub E, Ugurbil K, WU-Minn HCP Consortium (2013) The WU-Minn human connectome project: An overview. *Neuroimage* 80: 62–79.

Verret L, Mann EO, Hang GB, Barth AM, Cobos I, Ho K, Devidze N, Masliah E, Kreitzer AC, Mody I, Mucke L, Palop JJ (2012) Inhibitory interneuron deficit links altered network activity and cognitive dysfunction in Alzheimer model. *Cell* 149: 708–721.

Vitanova KS, Stringer KM, Benitez DP, Brenton J, Cummings DM (2019) Dementia associated with disorders of the basal ganglia. *J Neurosci Res* 97: 1728-1741.

Wang K, Liang M, Wang L, Tian L, Zhang X, Li K, Jiang T (2007) Altered functional connectivity in early Alzheimer's disease: a resting-state fMRI study. *Hum Brain Mapp* 28: 967–978.

Wang L, Zang Y, He Y, Liang M, Zhang X, Tian L, Wu T, Jiang T, Li K (2006) Changes in hippocampal connectivity in the early stages of Alzheimer's disease: evidence from resting state fMRI. *Neuroimage* 31: 496–504.

Wang P, Kong R, Kong X, Liégeois R, Orban C, Deco G, van den Heuvel MP, Thomas Yeo BT (2019) Inversion of a large-scale circuit model reveals a cortical hierarchy in the dynamic resting human brain. *Sci Adv* 5: eaat7854.

Weible AP (2013) Remembering to attend: the anterior cingulate cortex and remote memory. *Behav Brain Res* 245: 63–75.

Wilson HR, Cowan JD (1972) Excitatory and inhibitory interactions in localized populations of model neurons. *Biophys J* 12: 1–24.

Wu Y, Lin W, Shen D, Yap PT and UNC/UMN Baby Connectome Project Consortium (2019) Asymmetry spectrum imaging for baby diffusion tractography. In *International Conference on Information Processing in Medical Imaging* (pp. 319-331). Springer, Cham.

Wu Y, Hong Y, Feng Y, Shen D, Yap PT (2020) Mitigating gyral bias in cortical tractography via asymmetric fiber orientation distributions. *Medical Image Analysis* 59: 101543.

Wu Z, Guo Z, Gearing M, Chen G (2014) Tonic inhibition in dentate gyrus impairs long-term potentiation and memory in an Alzheimer's disease model. *Nat Commun* 5: 4159

Xu Y, Zhao M, Han Y, Zhang H (2020) GABAergic inhibitory interneuron deficits in Alzheimer's disease: implications for treatment. *Front Neurosci* 14: 660.

Yan CG, Zang YF (2010) DPARSF: A MATLAB Toolbox for "Pipeline" Data Analysis of Resting-State fMRI. *Front Syst Neurosci* 4: 13.

Yeo BT, Krienen FM, Sepulcre J, Sabuncu MR, Lashkari D, Hollinshead M, et al. (2011) The organization of the human cerebral cortex estimated by intrinsic functional connectivity. *J Neurophysiol* 106: 1125–1165.

Yuan P, Grutzendler J (2016) Attenuation of b-amyloid deposition and neurotoxicity by chemogenetic modulation of neural activity. *J Neurosci* 36: 632–641.

Zalesky A, Fornito A, Bullmore ET (2010) Network-based statistic: identifying differences in brain networks. Neuroimage 53: 1197-1207.

Zhang HY,Wang SJ, Xing J, Liu B, Ma ZL, Yang M, Zhang ZJ, Teng GJ (2009) Detection of PCC functional connectivity characteristics in resting-state fMRI in mild Alzheimer's disease. *Behavioural Brain Research* 197: 103–108.

Zimmermann J, Perry A, Breakspear M, Schirner M, Sachdev P, Wen W, Kochan NA, Mapstone M, Ritter P, McIntosh AR, Solodkin A (2018) Differentiation of Alzheimer's disease based on local and global parameters in personalized Virtual Brain models. *Neuroimage Clin* 19: 240-251.

Zott B, Busche MA, Sperling RA, Konnerth A (2018) What happens with the circuit in Alzheimer's disease in mice and humans? *Annu Rev Neurosci* 41: 277-297.